Division of Engineering
BROWN UNIVERSITY
PROVIDENCE, R. I.

METHODS OF IMPROVING THE EFFICIENCY OF PHOTOVOLTAIC CELLS

Eighth Semiannual Report

September 1, 1973 - February 28, 1974

J. J. Loferski
B. Roessler
E. E. Crisman
L. Y. Chen
R. Kaul

National Aeronautics and Space Administration
Washington, D. C.

NASA Grant NGR 40-002-093

METHODS OF IMPROVING THE EFFICIENCY OF PHOTOVOLTAIC CELLS

Eighth Semiannual Report on

NASA Grant NGR 40-002-093

September 1, 1973 - February 28, 1974

BROWN UNIVERSITY
Division of Engineering
Providence, Rhode Island 02912

J. J. Loferski
B. Roessler
E. E. Crisman
L. Y. Chen
R. Kaul

Sponsored by: National Aeronautics and Space Administration

Washington, D. C.

Abstract

The report summarizes work done in two areas during the period September 1, 1973 through February 28, 1974. The first of these is a continuation of work on aluminum-alloyed silicon grating cells. Work on optimization of the geometry (grating line width and spacing) confirms the previously presented analysis of such cells. A 1 cm^2 grating cell has been fabricated and its i-V characteristic has been measured under an AMO solar simulator; it is found that the efficiency of this cell would be about 7.9% if it were covered by the usual anti-reflection coating. Note that the surface of the cell is not covered by a diffused junction. The response is blue shifted; the current is somewhat higher than that produced by a commercial Si cell. However the open circuit voltage is low and attempts to optimize the open circuit voltage of the aluminum-alloy junctions are described. The second area of investigation is a preliminary X-ray topographic examination of GaAs specimens of the type commonly used to make solar cells. The X-ray study shows that the wafers are "filled" with regions having strain gradients, possibly caused by precipitates. It is possible that a correlation exists between the presence of low mechanical perfection and minority carrier diffusion lengths of GaAs crystals.

Table of Contents

I. INTRODUCTION

This report consists of two parts. The first describes the current status of the work on grating cells, i.e., photovoltaic cells made by producing a fine grating-like pattern of minority carrier collectors on the light receiving surface of a semiconductor crystal. In the experiments reported here, the semiconductor is single crystal silicon. The collectors are formed by alloying a grid of fine aluminum lines into the silicon. The second part of the report describes the status of an X-ray topographic examination of some GaAs single crystal wafers of the type commonly used to make GaAs photovoltaic cells by diffusion or by epitaxial techniques.

II. ALUMINUM-SILICON ALLOY JUNCTION GRATING PHOTOVOLTAIC CELLS

a) Fabrication Procedure and Open Circuit Voltage (V_{oc})

In our last report we described our procedure for fabrication of aluminum-silicon alloy junction grating cells. The following steps are followed in making these cells.

1) The "as-received" silicon wafer having resistivity in the range 0.1 to 10 ohm cm is cleaned in accordance with standard procedures commonly used for fabrication of microelectronic circuits. [(i) The wafer is cleaned ultrasonically in trichloroethylene for 30 sec, followed by cleaning in acetone for 30 sec. and in methanol for 30 sec. (ii) It is washed in a 1:1:5 solution of NH_4oH, H_2O_2 and deionized H_2O at 80°C for 15 min. (iii) It is washed in a 1:1:6 solution of HCℓ, H_2O_2 and deionized H_2O for 15 min. (iv) It is rinsed in deionized H_2O. (v) It is dipped in buffered HF for 20 sec.].
2) A thin layer of aluminum (about 7000Å) is deposited on the clean (polished) surface by vacuum evaporation.
3) Two thin layers, the first of titanium and the second of silver, are deposited on the other side of the silicon wafer. (After "suitering" this two layer combination makes an ohmic contact to the silicon wafer.)

4) A layer of A-Z positive photoresist is spread over the aluminum covered surface.

5) The photoresist is exposed through a mask which defines the grating pattern or patterns.

6) The photoresist is developed with A-Z developer. It happens that the developer removes both the photoresist and the aluminum from the regions which are intended to be the spaces between the lines in the grating pattern. The material in these spaces is "virgin silicon", i.e., the base wafer material.

7) The remaining photoresist is removed by dissolving in acetone, thus leaving behind on the wafer an aluminum pattern of the desired form.

8) The wafer is heated in a reducing atmosphere at temperatures in the vicinity of, or above, the silicon-aluminum eutectic temperature (576°C). During the heating process the aluminum alloys with the silicon forming p-n junctions and the Ti-Ag layers form an ohmic contact to the base.

9) Leads are attached by bonding Cu wires with "silver print" paint to the Aℓ on the light receiving surface of the cell.

The particular samples to be discussed here were made from silicon having a resistivity between 2 and 3.5Ω cm and a (100) surface on which the aluminum pattern was to be formed. Our first goal was to continue the exploration of alloying temperatures and schedules in the hope that open-circuit voltages (V_{oc}) higher than those reported in our last semiannual report[1] (0.44V) could be obtained if the alloying process were optimized. Toward this end we prepared a group of samples having the configuration shown in Fig. 1. Twenty-one sets of three units were prepared from each silicon wafer. After the pattern had been defined (as in step #7 above) each of the samples was subjected to two kinds of alloying schedules. In one of these the samples were heated "slowly" in the other, "rapidly". In the

[1]Seventh Semiannual Report - NASA Grant NGR 40-002-093, Brown University, Division of Engineering - September 1 through February 28, 1973.

rapid heating experiments, the controller of the furnace was set at the desired temperature and the furnace was turned on. It was found that with our combination of furnace and controller, (the controller used in these experiments is capable of causing more rapid heating than the one used in the experiments reported in our previous report) the interior of the furnace could reach a temperature in the vicinity of 700°C in about five minutes; samples subjected to this faster heating schedule were construed to have undergone "rapid" heating. [This "rapid" heating cycle is to be contrasted with cycle (a), the fast heating cycle defined in our previous report. In that case, the furnace was brought up to the desired temperature and the sample was shoved into the hot furnace; the heating from room temperature to 700°C occurred in a minute or less.] In the "slow" heating experiments, the controller setting was gradually increased up to the desired temperature; about 15 minutes were consumed in attaining 700°C. [This is similar to the slow heating cycle (b) of our previous report.]

In either case, the procedure was as follows. The sample was placed inside a quartz tube which passed through the tubular furnace; the sample was positioned so that it would be in the middle of the two foot long furnace. With the furnace at room temperatue, the quartz tube was sealed. It was purged with N_2 gas for 15 minutes followed by H_2 for 15 minutes before the furnace was turned on. The H_2 continued to flow through the tube during the heating cycle until the temperature in the furnace had returned to room temperature.

In both the rapid and slow heating cycles, the furnace was shut off as soon as the furnace had reached the desired processing temperature, i.e., the sample was kept at its maximum temperature for a few minutes only.

The open circuit voltage (V_{oc}) was measured by exposing the cells to light from a tungsten iodide source coupled with a water filter intended to reduce the infrared content of the incident light. The intensity was about 100mW/cm^2, the

samples were measured in succession at the same position. The measurement was performed quickly, i.e., before the sample temperature could experience any increase. The experiments were mainly useful for comparing junctions of this group to each other rather than for comparing with the cells described in our previous report. Obviously, the aluminum covered "squares" of Fig. 1 are opaque; the photovoltage is generated because carriers produced within a diffusion length L of the periphery of the junction can be collected. Now

$$V_{oc} \sim \frac{Akt}{q} \ell n \frac{I_{sc}}{I_o} \qquad (1)$$

where I_{sc} is the short circuit current; I_o is the reverse saturation current, and A is an empirical parameter which has the value "2" for silicon junctions. The parameter I_{sc} is a function of the minority carrier diffusion length. Our goal in these experiments is to determine how I_o (and perhaps A) are affected by processing procedures. As we have previously noted, the solubility of Aℓ in silicon is so high that one would expect values of I_o and A comparable to that observed in diffused junctions. The fact has been, however, that whereas V_{oc} has a value of about 550 mV for AMO in such diffused jucntions, we have found consistently lower values in the Aℓ grating photovoltaic cells; Fig. 2 is a plot of V_{oc} as a function of the processing temperature. The curve exhibits a broad maximum with V_{oc} values in the vicinity of 500 mV for alloying temperatures between 650 and 750°C. While this maximum represents an improvement over the 440 mV peak value of our previous report, it still is lower than the diffused junction value. One important conclusion can be made on the basis of these experiments: the lower values of V_{oc} reported for our grating cells in our previous report are not caused by the "grating" pattern since V_{oc} observed from "square" Aℓ junctions are essentially the same as those observed on grating cells. [A possible explanation for the lower values of V_{oc} in the grating is that I_o is increased by a large surface recombination com-

ponent contributed by the periphery of the grating junction. The periphery of the "square" Aℓ junctions of Fig. 1 totals 7,000 microns whereas the junction periphery for a grating cell (see Fig. 20 of our previous report) having 5μ lines spaced 100μ apart (Fig. 22 of that report) is 40,000 microns and for 5μ lines spaced 40μ apart (Fig. 21 of that report) is 80,000μ. It was to explore the role played by junction "length" (i.e., periphery) that we fabricated these square junctions and studied their characteristics.] This conclusion is further supported by the observations we have made on the i-V characteristics of a 1 cm^2 grating cell as described below.

b) Optimization of Grating Geometry

In our last report, we described experiments aimed at maximizing the short circuit current by changes in the grating geometry. The results of that preliminary study indicated that the aluminum line width (2a) should be kept as small as possible and that the line spacing could perhaps be increased even beyond the maximum value explored up to that time (~95 microns). The optimum grating spacing should be a function of the minority carrier diffusion length L in the silicon wafer; the spacing should be of the order of L.

In this continuation of the experiment, cells of two different configurations were constructed by alloying aluminum gratings onto the (100) face of silicon wafers. One set of cells were constructed with a fixed line width (2a) and the spacing (2b) was varied. The line width was set at the minimum line width which we have been able to generate (about 5μ) and the spacing was varied between about 30 and 250 microns. The areas covered by the grating pattern were 50x50 $mils^2$ (1250x1250 $microns^2$). Six groups of three cells each were made on an n-Si wafer having ρ = 2 to 3.5 ohm cm. The actual values of 2a and 2b are given in Table 1. The second set maintained a fixed line width to line spacing (a/b) ratio: the value chosen was a/b = 3. Six values of line width were used; nine groups of cells were made. Group 9 consisted of a 50x50 mil^2 "picture frame", i.e., no grating pattern covered the surface. Groups 7 and 8 have the same grating structures as

Groups 2 and 4, respectively; however, the former also have four grating lines at right angles to the main grating pattern. The actual values of 2a and 2b are given in Table 2.

These cells were fabricated according to the rapid heating cycle described in Section (a). The short circuit currents I_{sc} of these cells were measured for each of these cells exposed to a tungsten iodide lamp. The light intensity was set at a value which resulted in a short circuit current density of 26.3 mA/cm^2 from a 2 cm^2 "common-variety" commercial silicon solar cell whose anti-reflection coating has been removed by etching in buffered HF. The highest values of short circuit current for each of the groups are recorded in Tables 1 and 2.

The following conclusions can be offered at this time. For a fixed line width (Table 1), the value of I_{sc} passes through a maximum. On the low spacing side, response drops off because the fraction of the surface covered by the opaque aluminum grating lines increases. Thus, when the spacing is 31.8μ, about 15% of the surface is covered by Aℓ. When the spacing is 127.2μ, about 4% of the surface is covered by Aℓ. Therefore, the current for the grating with larger spacing should be larger by about 10% than the current for the smaller spacing. According to the data, the ratio of the currents from the 31.8μ to the 127.2μ spacings is about 0.89. On the high spacing side of the maximum the current drops off because the spacing becomes large compared to a diffusion length.

For a fixed a/b ratio, the same fraction of the base wafer is always absorbing the light. The observed decrease in I_{sc} occurs because the dependence of I_{sc} on the ratio of spacing to diffusion length. These data have yet to be analyzed more thoroughly.

c) Measurement on a 1 cm^2 Grating Cell

We fabricated a 1 cm^2 grating cell on a 2 to 3.5 ohm cm, (100) plane of a silicon wafer using the rapid heating cycle described above. The grating pattern consisted of 7.5μ lines spaced 127.2μ apart. The output of the cell was measured

under a Spectrolab artifical sun at the NASA Lewis Space Flight Center*. The intensity was set at 136 mW/cm^2 and the spectral distribution is a good approximation to the AMO spectrum. The i-V curve of this cell is shown in Fig. 3, which also includes the i-V curve of a 2 cm^2 commercial Si cell whose anti-reflection coating has been removed by dipping in HF. (The current reading for the 2 cm^2 cell has been reduced to current/unit area.)

The following points can be made. The 1 cm^2 grating cell produces a short circuit current comparable to indeed a little greater than that produced by this commercial cell. (With an anti-reflection coating, this cell should produce an I_{sc} about 1.4 times the uncoated cell values.) However, the open circuit voltage of the grating cell (0.47V) is smaller than that generated by the diffused junction cell (0.55V). The maximum power point for this 1 cm^2 grating cell occurs at 0.34V and 22.5mA; this corresponds to an efficiency of about 7.9%. The commercial cell of Fig. 3 has a maximum efficiency of about 11%. Thus we have shown that we can make a 1 cm^2 solar cell of about 8% efficiency without diffusing a junction over the whole surface of the cell. If we are able to decrease I_o and thus increase V_{oc} we should be able to at least equal the output of standard Si cells. Because the grating cell has a somewhat greater short circuit current, it is potentially a higher efficiency cell.

Figure 3 compares the spectral response of the 1 cm^2 grating cell to the spectral response of the commercial silicon cell whose i-V curve is given in Fig. 2. Note that the grating cell has a higher blue response. Note also that the Spectrolab AMO simulator is deficient in the blue compared to the true solar AMO spectrum. This means that I_{sc} for this grating cell exposed to true solar AMO illumination should be even larger compared to the commercial cell than is shown in Fig. 3.

---

*We wish to thank Dr. Henry Brandhorst of NASA Lewis, who made arrangements for these measurements and helped to perform them.

III. X-RAY TOPOGRAPHIC EXAMINATION OF SOME GaAs SINGLE CRYSTAL INTENDED FOR USE IN SOLAR CELLS

In an earlier report[2], we showed how X-ray topography could be used to exhibit changes in the defect content of silicon wafers subjected to the diffusion process. The contrast variations observed in X-ray topographs are related to regions in which there are strain gradients. Since dislocations and impurity precipitates have strain gradients in their vicinity, X-ray topographs can be used to determine the dislocation density and the extent to which precipitates may be present in a crystal. Variation in dislocation content can affect the minority carrier lifetime of germanium and silicon single crystals; precipitates can also be expected to affect this parameter which is so extremely sensitive to defects. We have therefore set out to use X-ray topographic techniques to guide us in the course of fabrication of GaAs cells. Our rationale is as follows. A "good" solar cell must require the longest possible minority carrier lifetime (i.e., diffusion length). All other things being equal, a crystal with a low dislocation content and a minimum of precipitates should have the highest lifetime. This is really a hypothesis. In the case of GaAs we really need to establish that mechanical perfection, i.e., the absence of defects giving rise to strain gradients, is correlated with high lifetime. This hypothesis has been partially verified in the case of silicon. Our approach to the silicon problem is therefore to start with strain-free (as demonstrated by X-ray topography) material and to subject it to successive stages in the fabrication of a solar cell (diffusion, contact formation, etc.). The material would be examined after each step to ascertain that its mechanical perfection had not been affected. Such a program makes sense in silicon.

However, knowledge of the role that mechanical perfection plays in controlling the minority carrier lifetime of GaAs is in a more rudimentary state.

---

[2] Sixth Semiannual Report - NASA Grant NGR 40-002-093, Brown University, Division of Engineering, September 1, 1973 - February 28, 1974. The X-ray topographic study was performed by Professor Barton Roessler and Mr. R. Kaul whose names were inadvertently left off that report.

What is known is that minority carrier diffusion length can vary over an order of magnitude in GaAs crystals containing the same concentrations of donors or acceptors, and grown under essentially the same conditions. Our first goal was therefore to subject some GaAs single crystals, intended for solar cells, to X-ray topographic examination. Two GaAs wafers have been examined to date. X-ray topographs indicate that all of them are "filled" with regions having large strain gradients. This is to be contrasted with silicon single crystals used in solar cells which contain a modest concentration of dislocations but have virtually no evidence of precipitates. The remainder of this report is concerned with details of the examination of these three specimens.

a) Specimen #2 was obtained from the Bell and Howell Electronic Materials Divison (Mr. Gil Walker of NASA-Langley provided this specimen and the other GaAs used in this study). It is zinc doped, p-type material; the resistivity is in the 1-10 ohm cm range. The specimen is tear-drop shaped with a straight edge (for orientation in subsequent fabrication) in the $[\bar{1}10]$ direction. X-ray back reflection photographs showed that the surface is (001). Visual examination showed that one surface of the specimen is flat and specular--characteristic of a well-polished surface and the second surface has a rough, dull surface which is probably the surface condition characteristic of a prior cutting or coarse polishing operation.

Several (220) X-ray topographs have been recorded using Mo radiation. The crystal thickness is approximately 0.012 inches thick. The product of the linear absorption coefficient, μ_o, and the thickness, t_o, is approximately 6.0; the crystal, accordingly, is "thick" in the X-ray sense and the X-ray topographs are obtained by the anomalous transmission phenomenon. Dislocation images are--consequently--regions of reduced X-ray intensity.

Figure 5 shows a low magnification (18x) topograph (L-131) obtained with the X-rays incident upon the rough, non-specular surface. The mottled appearance

of the surface was attributed to the redistribution of the X-ray intensity in the surface damaged layers upon which the X-ray beam is incident. The details in the images in the region at the bottom of Fig. 5 are shown at higher magnification in Fig. 6.

We assumed that the surface damage obviously present in the abraded surface was obscuring our view. This could occur when the X-ray beam was incident upon the rough, nonspecular surface on the abraded side of the GaAs specimen. Since this mottled appearance was similar to that observed previously in the topographs recorded from silicon specimens with a similarly rough surface, it was expected that chemical polishing would remove this surface damage and that the topographs would then show dislocations and other imperfections in the crystal more clearly as was the case for the silicon specimen.

Accordingly, the GaAs wafer was chemically polished in an H_2O_2-H_2SO_4 solution. Contrary to our expectations, this chemical polishing procedure did not produce flat smooth surfaces on the specimen. Instead, both surfaces -- the formerly smooth specular "front" surface the formerly rough abraded "back" surface -- developed a series of deep troughs and grooves that looked very much like the remnants of old deeply damaged areas due to previous scratches introduced during some prior polishing procedure. Both surfaces, though not flat, were extremely shiny, i.e., had a metallic luster.

Figure 7 is an optical reflected-light photograph at a magnification of about 8x of the formerly smooth (front) surface after the H_2O_2-H_2SO_4 chemical polish. It shows the series of deep troughs that were, in fact, visible on both surfaces. Figure 8 shows this same surface using ordinary reflected-light optics in oblique illumination at a magnification of 18x and indicates that the surface irregularities were so deep that the depth of field was insufficient to permit focusing on the surface. The cell-like network that is seen in Fig. 8 shows

that the chemical polish has not removed the surface layers uniformly. It is likely that boundaries of these cells have been more rapidly attacked by the chemical polish than the cell interiors as a result of non-uniformity in the composition of the crystal. Some of the deep grooves in Fig. 7 appear to be due to surface damage from previous polishing operations since they have the appearance of rather long straight lines, i.e., like scratches. It should be recalled, in this connection, that the condition, before chemical polishing, of the surface shown in Figs. 7 and 8 was that of the as-received crystal -- a specular, lustrous surface with no easily discernible scratches. If the long straight lines shown in Figs. 7 and 8 reveal damage due to prior precessing, the damage extends well below the original "as-received" surface. The chemical polish, then, did not polish uniformly and, in fact, seems to resolve what may be impurity segregation at cell boundaries as well as scratch damage deep in the crystal.

Figure 9 is a (220) X-ray topograph [L162 (LP154, LP155)] of the crystal in this chemically-polished condition. The region at the top of Fig. 9 is shown at higher magnification in Fig. 10. The white angular lines at D may be dislocation images or may be a diffraction effect at the cell boundaries. Regardless of the interpretation of the diffraction effects shown in Fig. 10, it is clear that the chemical polishing procedure did not do what was expected, i.e., remove the damage in the abraded back surface of the as-received crystal and leave flat, smooth, specular surfaces suitable for X-ray topography.

We then proceeded to mechanically polish the back surface (now deeply grooved but shiny) to a flat specular surface so as to eliminate shadowing in the X-ray topographs due to the surface irregularities. The specimen was polished with 9μm, 1μm and then 0.3μm Al_2O_3 using deionized distilled water as a lubricant. The crystal thickness after this procedure was 0.010 inches. (The thickness of the as-received specimen was 0.0135 inches.)

Visual examination of this flat specular surface showed that it was full of many small holes. This could be seen with the naked eye in oblique illumination and is shown in Fig. 11 (Met 30 and 31). At higher magnification it appears that a second phase particle has been pulled out of the crystal by the polishing procedure to form these holes. It was confirmed by focusing (at high magnification (800x)) up and down, that they were, in fact, holes and not particles embedded in the matrix and protruding from the surface. A Nomarski interference contrast photograph of this mechanically polished surface is shown in Fig. 12 (Met. 36). Surface scratches from the mechanical polish are now easily seen in addition to the holes. It should be pointed out that it is not possible using bright field illumination to observe these surface features anywhere near as clearly as when Nomarski contrast is used. This fact is illustrated by Figs. 13 and 14 which compare the identical region on the original as-received specular surface of GaAs #2 in ordinary bright field reflected light (Fig. 13) and in Nomarski contrast (Fig. 14). A flat specular surface is not, then, a damage-free surface.

The central feature of these results is that the quality -- in the sense of crystalline perfection -- of GaAs Specimen #2 is low. Both X-ray topography and optical microscopy suggest that the crystal contains second phase particles and/or substantial polishing damage. The Ga-As-Zn ternary phase diagram [see Fig. 7, p.68, "The Use of the Phase Diagram in Investigations of the Properties of Compound Semiconductors", M. B. Panish, in Phase Diagrams: Materials Science and Technology 6-III, Editor Allen M. Alper, Academic Press (1970)] indicates the segregation effects which will occur during solidification. As the melt solidifies one may expect constitutional undercooling effects and a resulting cellular structure to form [see, for example, "Solidification Structures of Solid Solutions", by L. A. Tarshis, J. L. Walter, and J. W. Rutter in ASM Metals Handbook, Vol. 8, p.150 (1973)]. The precipitation of other compounds, such as Zn_3As_2, may then be

expected (if their specific volumes are appropriate) to cause elastic strains at the cellular boundaries. Such precipitate associated strains have been shown [see Fig. 21 in "The Application of X-Ray Topographical Techniques to the Study of Semiconductor Crystals and Devices", by E. S. Meieran, Siemens Review, Vol. XXXVII, p.61 (1970)] to give an X-ray topograph which is similar to those presented in this report as Fig. 6 and 9. Since Meieran also presents X-ray topographs of GaAs in which individual dislocations are easily resolved, it seems reasonable to conclude that our GaAs Specimen #2 was not material of high crystalline perfection. The difficulties probably arise during the growth from a zinc doped melt.

It should be mentioned that the crystalline perfection of such doped melt grown crystals can apparently be quite good -- at least insofar as can be indicated by etch pitting procedures [see, A. G. Thompson, Journal of Electronic Materials, Vol. 2, p.47 (1973)].

b) Our second wafer was cut from a Si doped GaAs crystal. It has a rough abraded "back" surface and a smooth, specular (lustrous) front surface. X-ray topographic examination showed it to be too thick for reasonable exposure times using Ag radiation and so the crystal thickness was reduced from the as-received thickness of 0.014 in. to about 0.008 in. by mechanical polishing the back surface on 9μm, 3μm, and 0.3μm Al_2O_3. It was then chemically polished in $HF-HNO_3-H_2O$ 1:3:4 for two minutes.

A (220) X-ray topograph of this specimen is shown in Fig. 15 (LP218-L211). It shows this specimen to be of low quality similar to Specimen #2. A Nomarski interference contrast photograph of the front specular surface in the as-received condition is shown in Fig. 16 (Met. 42). It appears similar to the more extensively examined Specimen #2 and confirms that this specimen is also of low quality as compared to silicon or even as compared to what is possible with GaAs crystals.

IV. SUMMARY AND CONCLUSIONS

1. A $1cm^2$ alloyed aluminum silicon grating solar cell has been fabricated. Its current-voltage characteristic was measured using an AMO simulator. It was concluded that its AMO efficiency would be about 7.9% if the cell were covered by a standard antireflection coating.

2. A series of small area alloyed aluminum grating cells were fabricated and tested in a continuing attempt to optimize grating line-width, spacing and heat treatment. The "best" cells are made by alloying at temperatures around 700°C for a few minutes. Line spacings of about 100μ seem to result in the highest values of short circuit current in the silicon wafers used in the study. The minority carrier diffusion length in these wafers is therefore well in excess of 100μ.

3. X-ray topography studies of GaAs wafers of the kind commonly available for making solar cells indicates the presence of a large concentration of strain gradients. These crystal wafers are known to have low diffusion lengths (about 1μ).

V. PLANS FOR FUTURE WORK

1. Grating cells will be made on GaAs wafers by alloying Aℓ-Zn grating lines into single crystal GaAs wafers.

2. GaAs crystals which have diffusion lengths in the range of 10μ will be subjected to X-ray topographic examination.

3. Attempts will continue to correlate solar cell efficiency with strain gradients and mechanical imperfections in silicon and gallium areuide.

JJL/11t

Figure Titles

Figure 1 Test sample configuration.

Figure 2 Open circuit voltage versus alloying temperature.

Figure 3 Characteristic under simulated AMO illumination.

Figure 4 Relative spectral response.

Figure 5 The (220) topograph (L-131) of GaAs specimen #2 showing mottled appearance due to surface damage in surface upon which X-rays are incident. Magnification, 18x.

Figure 6 The region at B in Figure 2 at higher magnification. White lines correspond to reduced X-ray intensity. Magnification, 43.2x.

Figure 7 An optical reflected light photograph of the grooved surface which developed upon chemically polishing (H_2O_2 + H_2SO_4) the flat specular surface of the as-received GaAs wafer (Specimen #2). Mag. 8x. (Met. 28 and Met. 29)

Figure 8 Same surface of chemically polished GaAs surface at higher magnification. Depth of troughs is too great to permit focusing. Mag. 18x. Oblique illumination (Met. 27). Note network of cells.

Figure 9 A(220) X-ray topograph of GaAs #2 after chemical (H_2O_2 - H_2SO_4) polishing. LP 154 (top), LP 155 (bottom). Mag. 18x. L-162. Molybdenum radiation. X-rays incident upon "back" surface. Crystal thickness 0.010 in.

Figure 10 A (220) X-ray topograph from GaAs #2 after chemical (H_2O_2 - H_2SO_4) polishing. Mag. 43.2x (LP 163 L-162). Molybdenum radiation. X-rays incident upon "back" surface. Crystal thickness ≈0.011 in.

Figure 11 Reflected light photograph of mechanically polished surface of GaAs #2. Same magnification as Fig. 7. Oblique illumination. Mag. 8 (Met. 30 and 31).

Figure 12 Nomarski interference contrast photograph of mechanically polished surface of GaAs #2. Mag. 240x. (Met. 36)

Figure 13 Reflected light photograph of as-received specular surface of GaAs #2. Mag. 240x. (Met. 19)

Figure 14 Nomarski interference contrast photograph from identical region shown in Fig. 13. Mag. 240x (Met. 18)

Figure 15 A (220) X-ray topograph from GaAs Specimen #1 Si doped. Mag. 27x. (LP218-L211) silver radiation.

Figure 16 A Nomarski interference contrast photograph (Met 42) of the as-received front surface of GaAs Specimen #1. Mag. 240x.

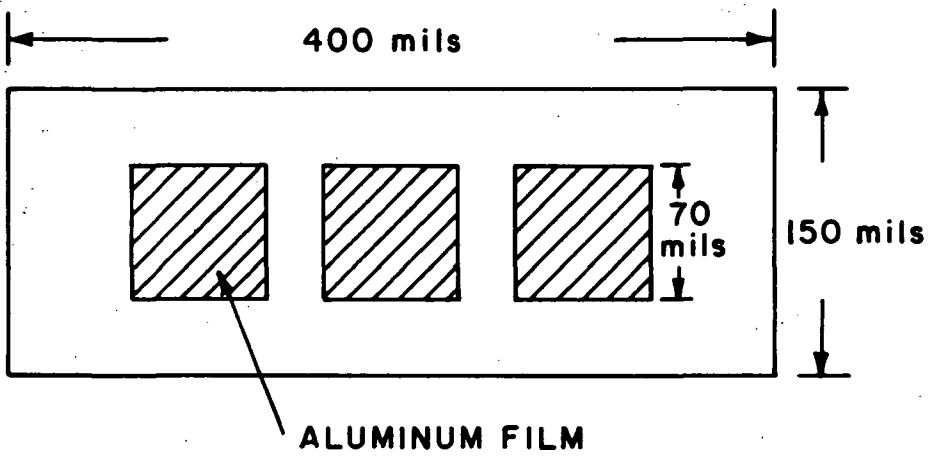

FIG. 1 TEST SAMPLE CONFIGURATION.

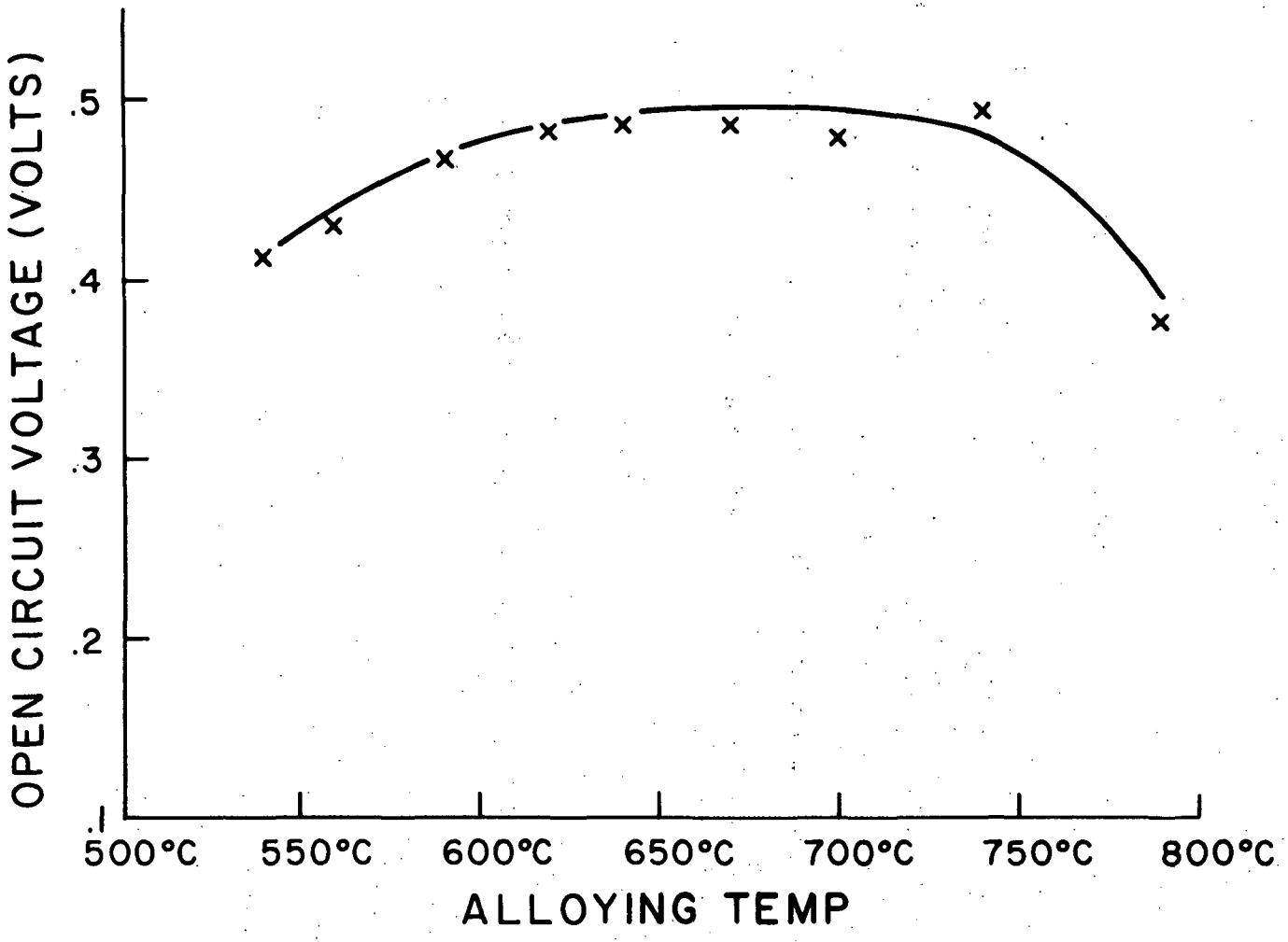

FIG. 2 OPEN CIRCUIT VOLTAGE VERSUS ALLOYING TEMPERATURE.

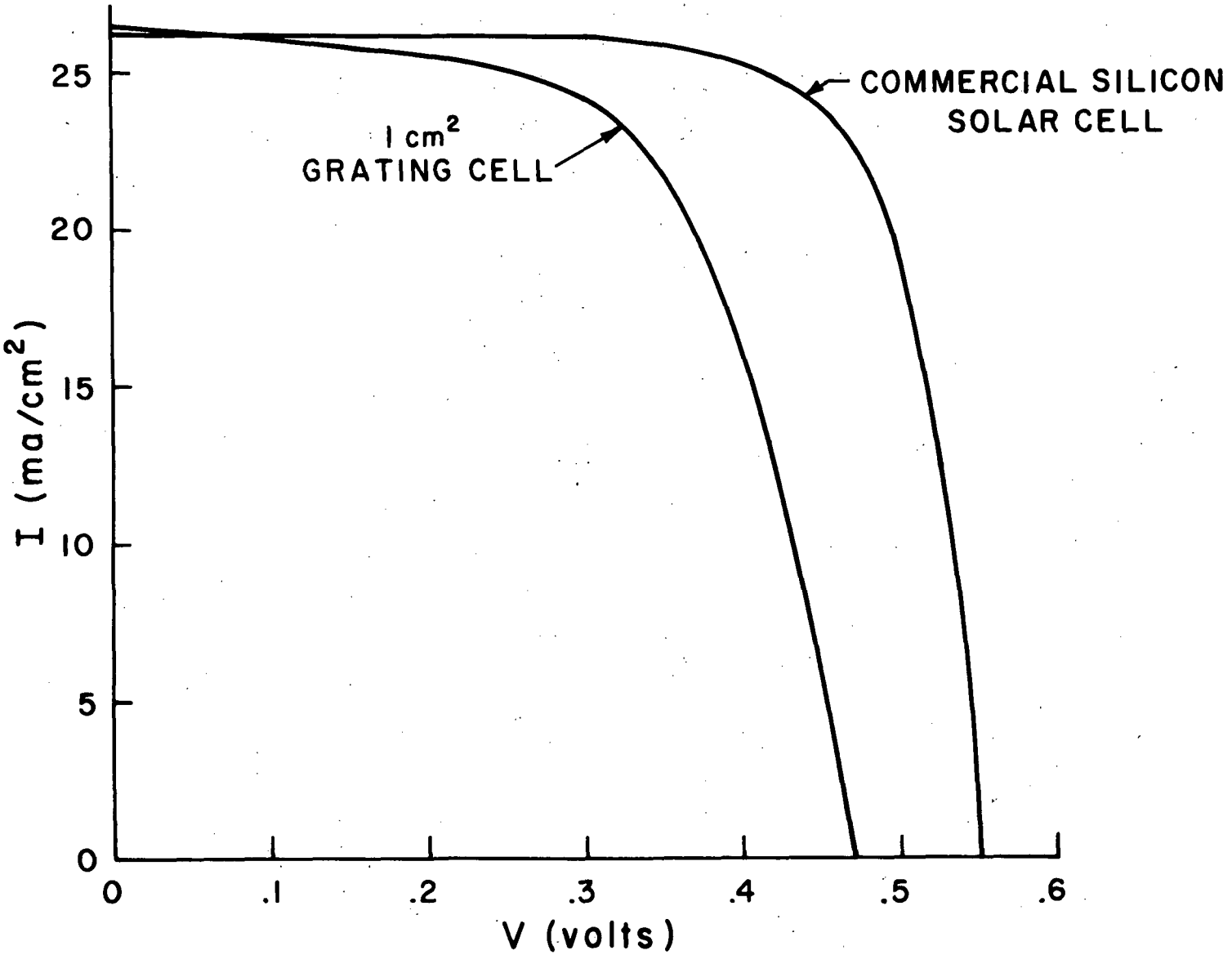

FIG. 3 CHARACTERISTIC UNDER SIMULATED AMO ILLUMINATION.

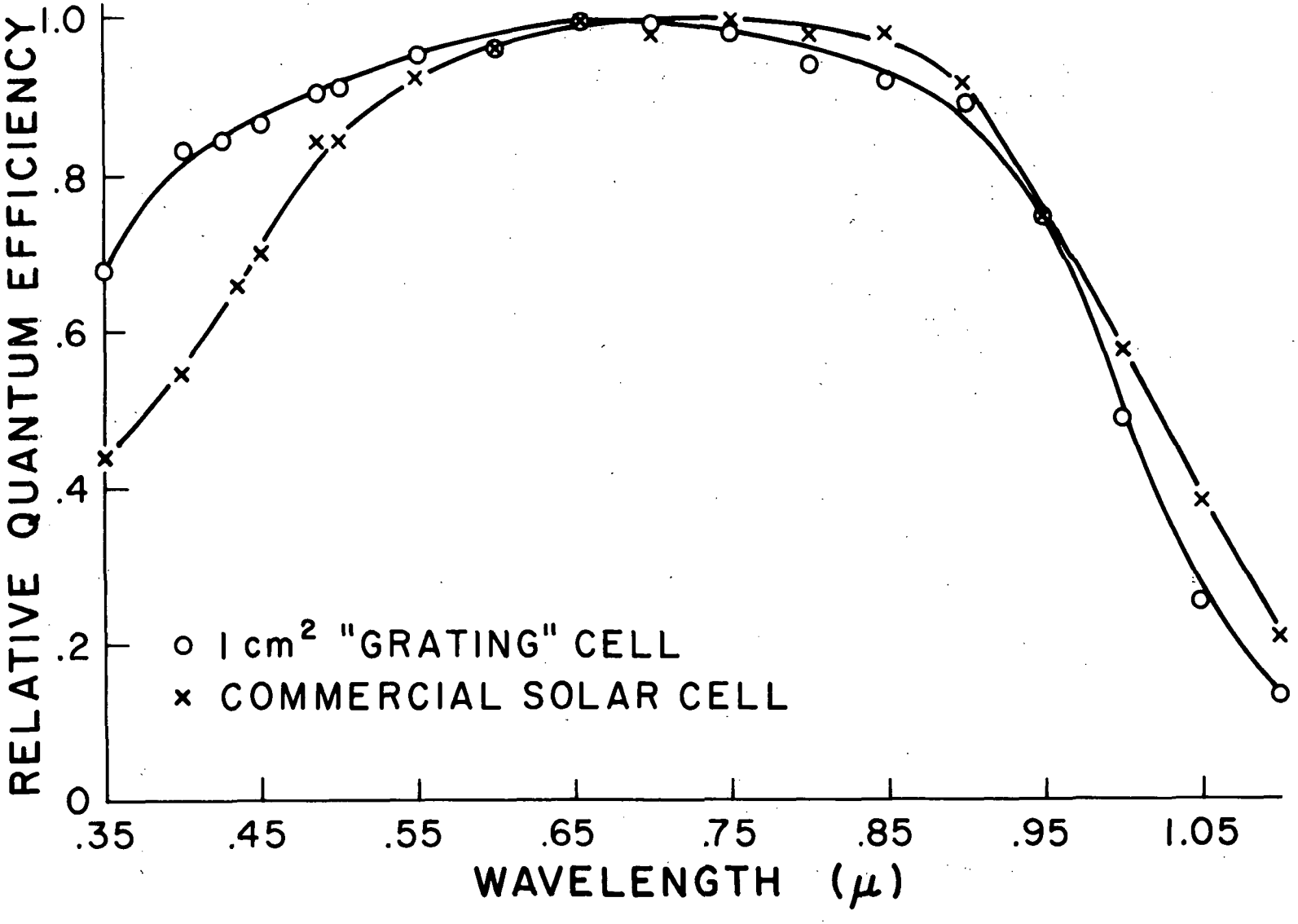

FIG. 4 RELATIVE SPECTRAL RESPONSE.

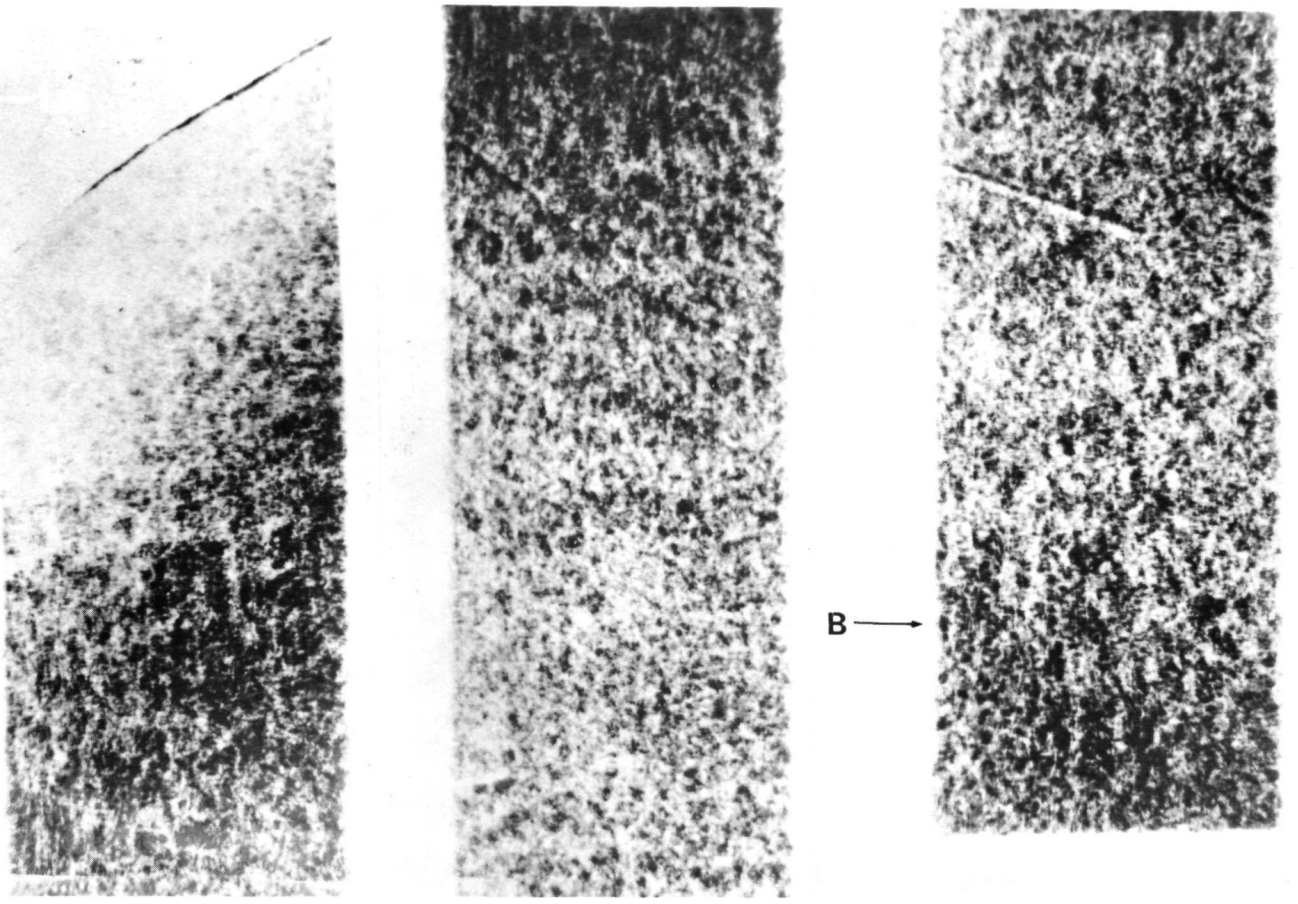

Fig. 5 The (220) topograph (L-131) of GaAs specimen #2 showing mottled appearance due to surface damage in surface upon which X-rays are incident. Magnification, 18×.

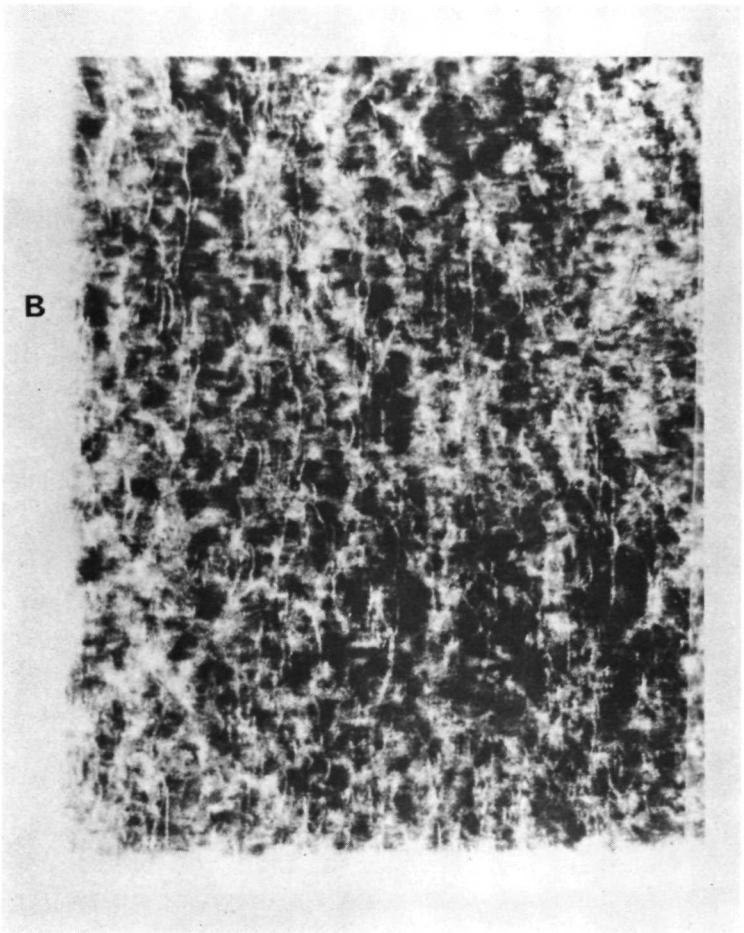

Fig. 6 The region at B in Fig. 2 at higher magnification. White lines correspond to reduced X-ray intensity. Magnification, 43.2×.

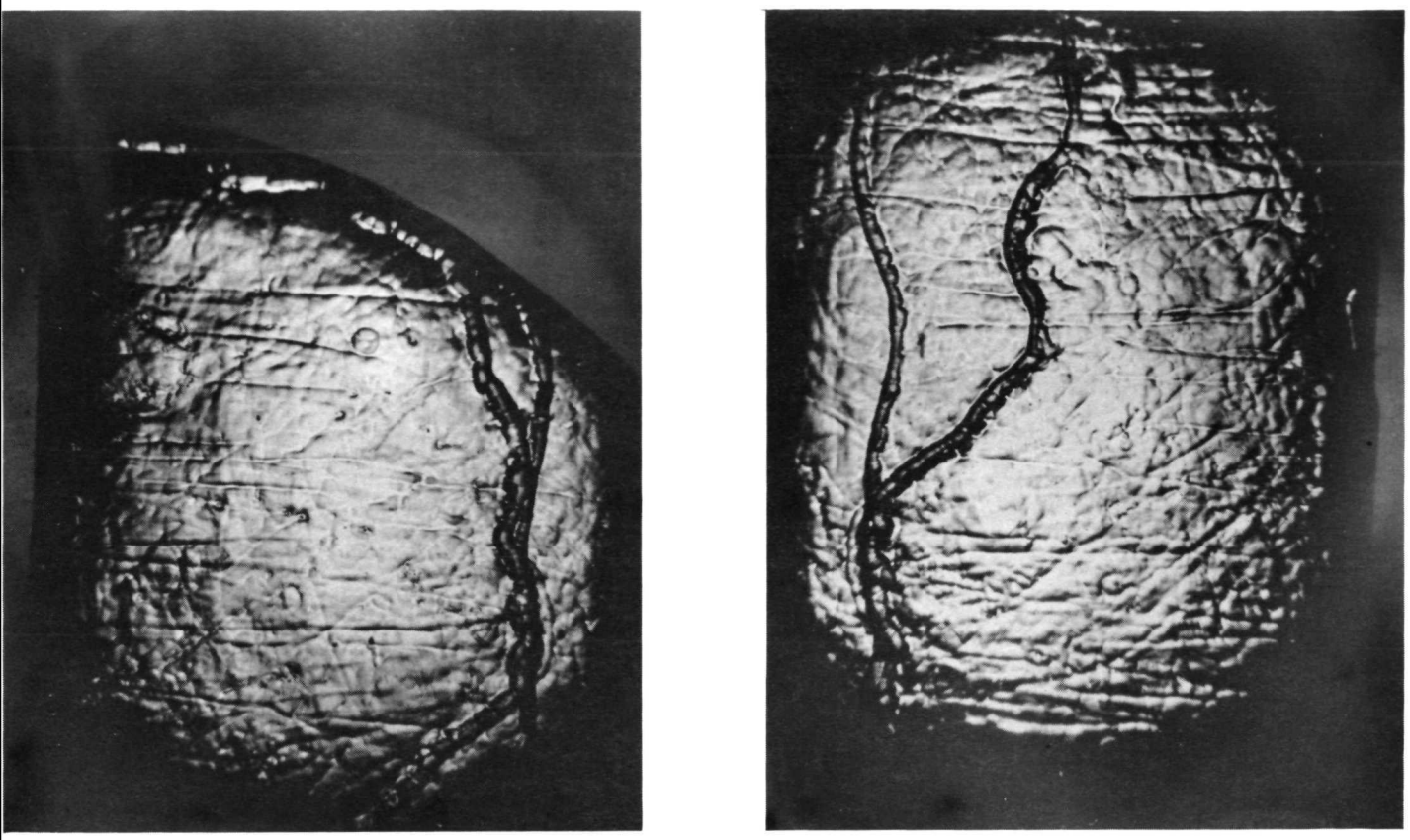

Fig. 7 An optical reflected light photograph of the grooved surface which developed upon chemically polishing (H_2O_2 + H_2SO_4) the flat specular surface of the as-received GaAs wafer (Specimen #2). Mag. 8×. (Met. 28 and Met. 29)

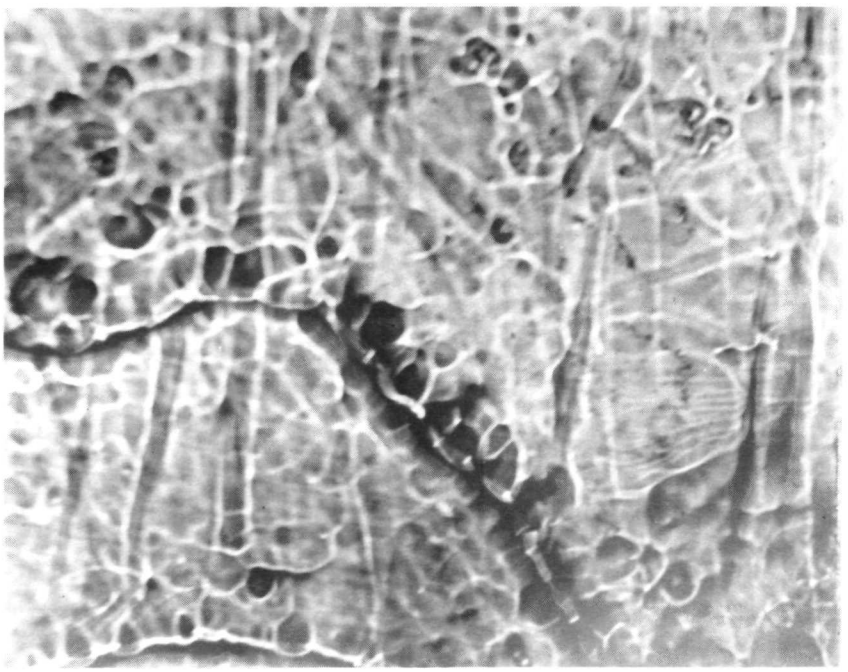

Fig. 8 Same surface of chemically polished GaAs surface at higher magnification. Depth of troughs is too great to permit focusing. Mag. 18×. Oblique illumination (Met. 27). Note network of cells.

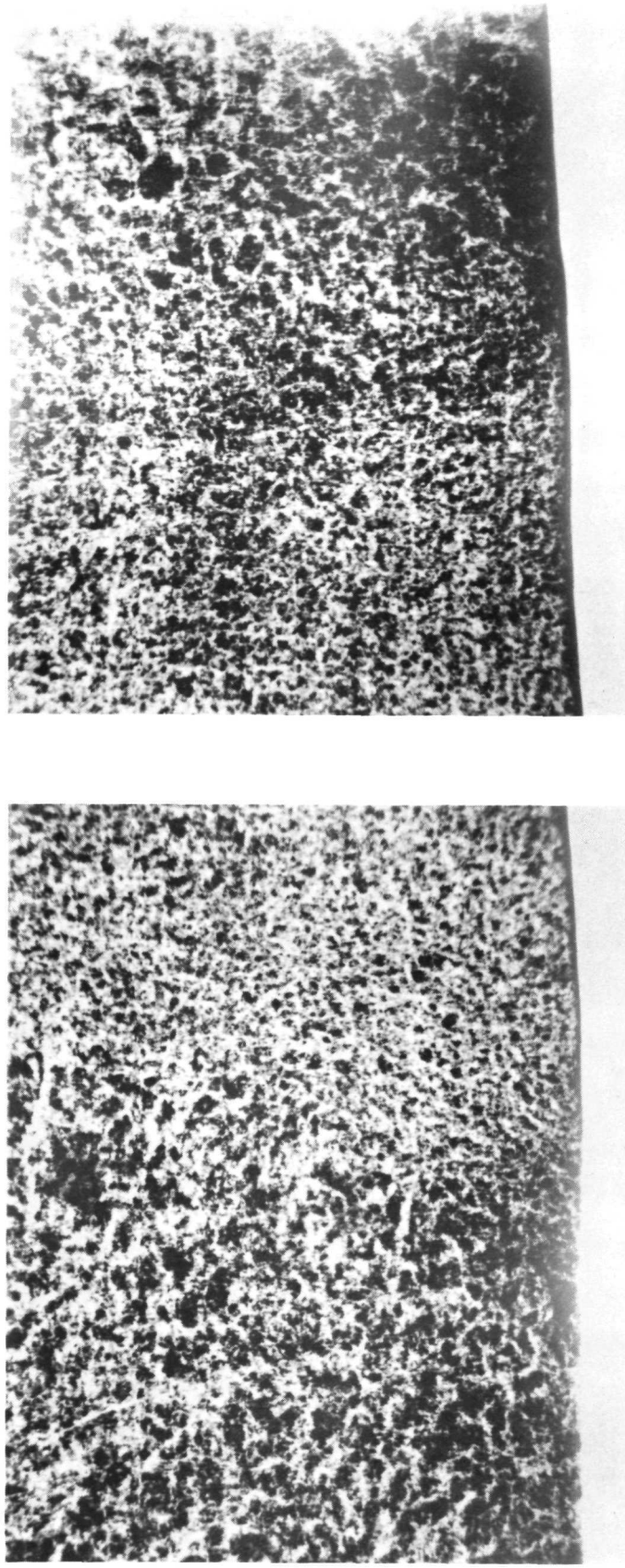

Fig. 9 A (220) X-ray topograph of GaAs #2 after chemical (H_2O_2 - H_2SO_4) polishing. LP 154 (top), LP 155 (bottom). Mag. 18×. L-162. Molybdenum radiation. X-rays incident upon "back" surface. Crystal thickness 0.010 in.

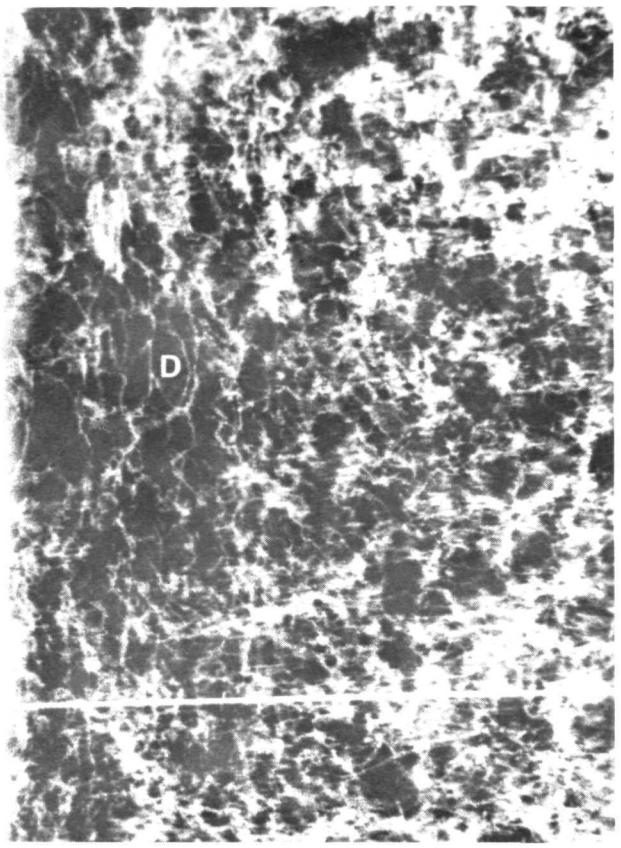

Fig. 10 A (220) X-ray topograph from GaAs #2 after chemical (H_2O_2 - H_2SO_4) polishing. Mag. 43.2× (LP 163 L-162). Molybdenum radiation. X-rays incident upon "back" surface. Crystal thickness ≈0.011 in.

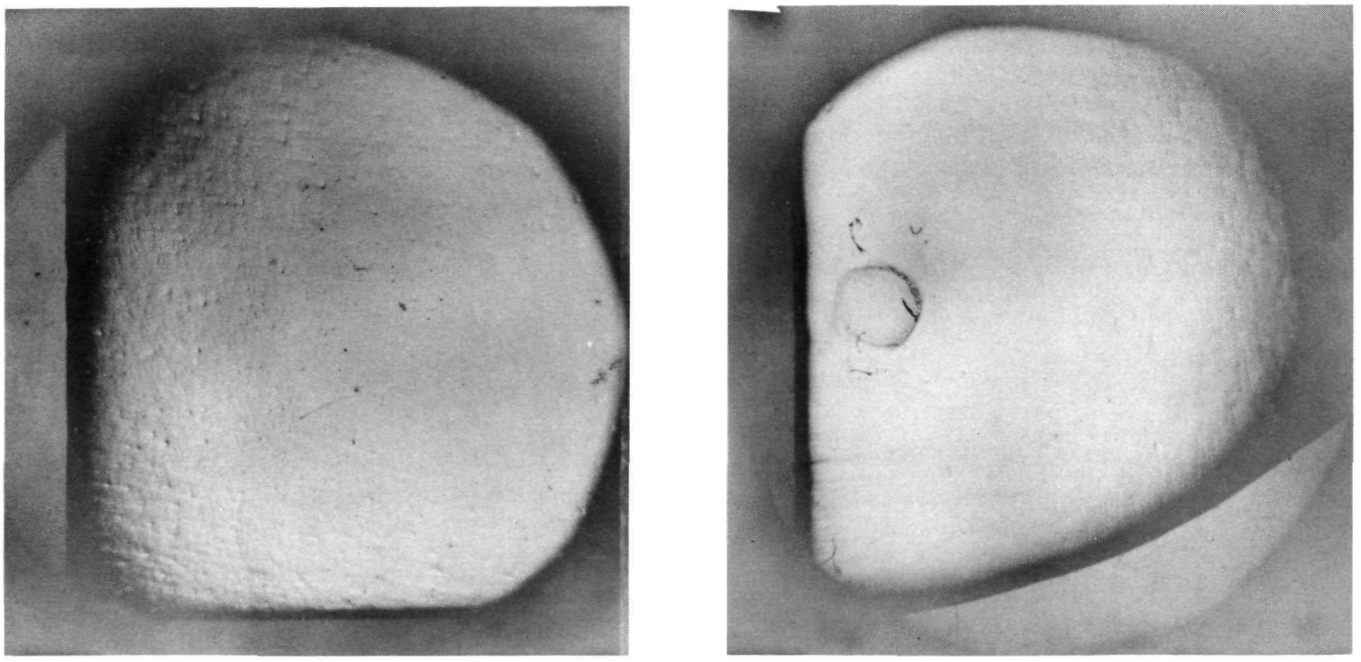

Fig. 11 Reflected light photograph of mechanically polished surface of GaAs #2. Same magnification as Fig. 7. Oblique illumination. Mag. 8 (Met. 30 and 31).

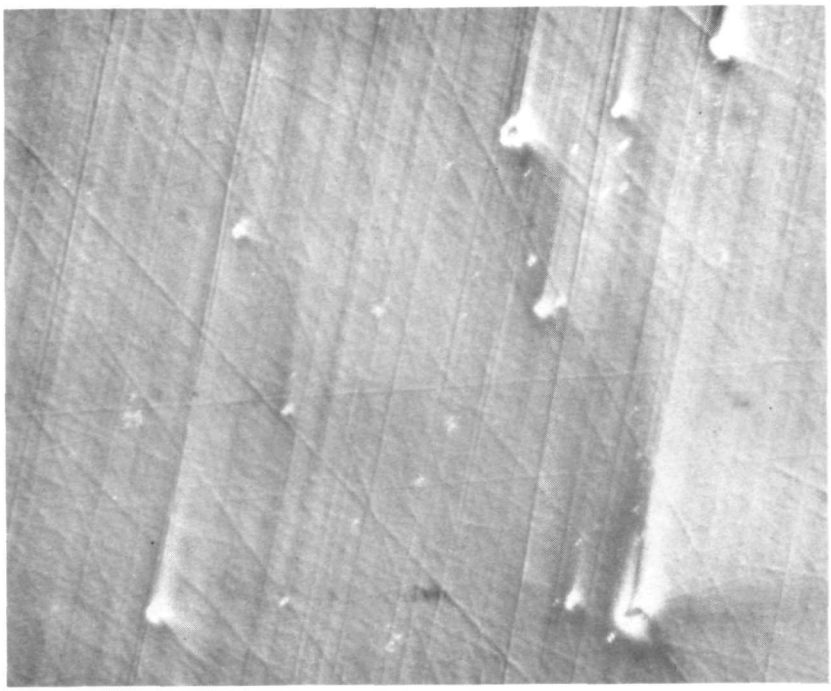

Fig. 12 Nomarski interference contrast photograph of mechanically polished surface of GaAs #2. Mag. 240×. (Met. 36)

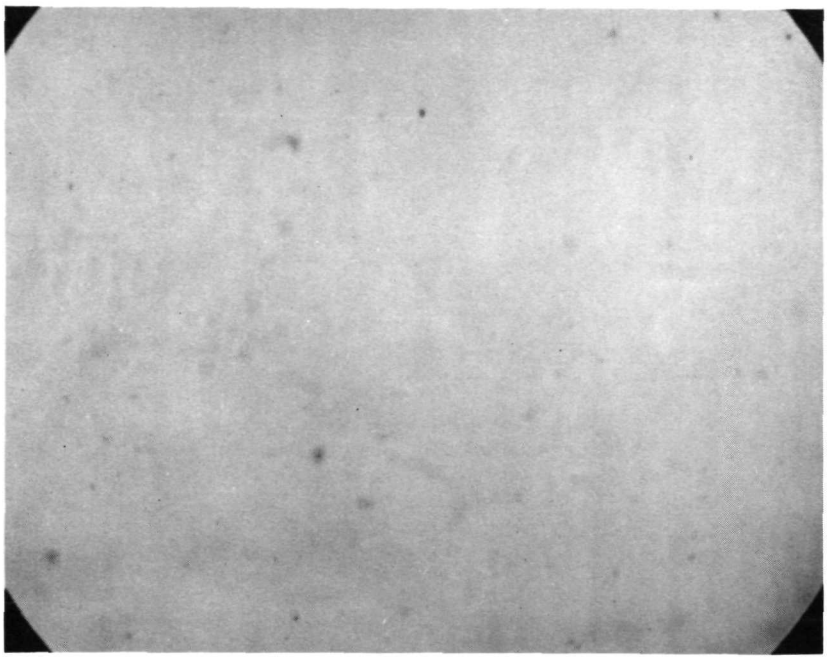

Fig. 13 Reflected light photograph of as-received specular surface of GaAs #2. Mag. 240×. (Met. 19)

Fig. 14 Nomarski interference contrast photograph from identical region shown in Fig. 13. Mag. 240× (Met. 18)

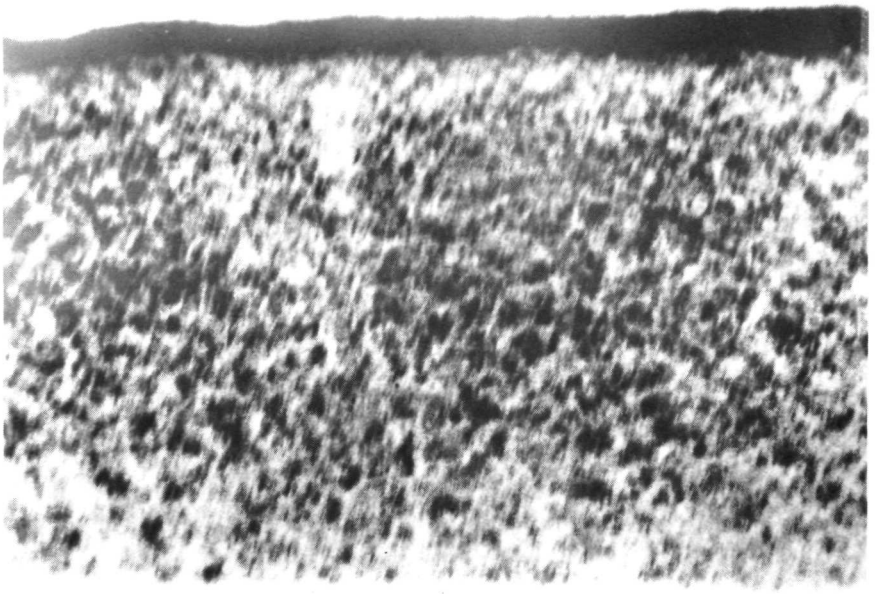

Fig. 15 A (220) X-ray topograph from GaAs Specimen #1 Si doped. Mag. 27×. (LP218-L211) silver radiation.

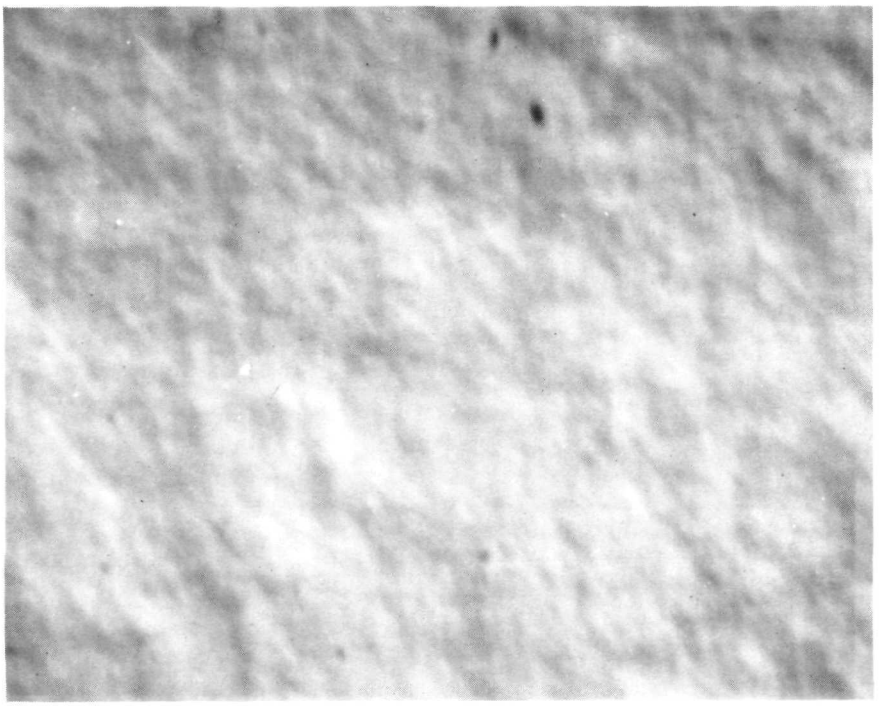

Fig. 16 A Nomarski interference contrast photograph (Met. 42) of the as-received front surface of GaAs Specimen #1. Mag. 240×.

TABLE 1

	Cell Nos.	Grating Line Width(2a) (μ)	Spacing(2b) (μ)	I_{sc}(ma/cm^2)
Group 1	1,7,13	5.1	31.8	24.7
Group 2	2,8,14	5.1	63.5	25.8
Group 3	3,9,15	5.1	95.3	25.6
Group 4	4,10,16	5.1	127.2	27.9
Group 5	5,11,17	5.1	190.8	26.8
Group 6	6,12,18	5.1	254.4	26.7

TABLE 2

	Cell Nos.	Grating Line Width(2a) (μ)	Spacing(2b) (μ)	I_{sc}(ma/cm^2)
Group 1	1,7,13	10.2	31.8	24.2
Group 2	2,8,14	20.4	63.6	22.7
Group 3	3,9,15	30.6	95.4	21.2
Group 4	4,10,16	40.8	127.2	21.9
Group 5	5,11,17	61.2	190.8	19.6
Group 6	6,12,18	81.6	254.4	19.3
Group 7*	19,22	20.4	63.6	19.7
Group 8*	20,23	40.8	127.2	16.6
Group 9	21,24			8.4